CHIN. PHYS. LETT. Vol. 37, No. 11 (2020) 117101

Distinct Three-Level Spin–Orbit Control Associated with Electrically Controlled Band Swapping

Yu Suo(索育)[1,2†], Hao Yang(杨浩)[1†], and Jiyong Fu(付吉永)[1,3,4*]

[1]*Department of Physics, Qufu Normal University, Qufu 273165, China*
[2]*Department of Physics, Jining University, Qufu 273155, China*
[3]*Instituto de Física, Universidade de Brasília, Brasília-DF 70919-970, Brazil*
[4]*Collaborative Innovation Center of Light Manipulations and Applications, Shandong Normal University, Jinan 250358, China*

(Received 1 July 2020; accepted 23 September 2020; published online 8 November 2020)

We investigate the Rashba and Dressehaus spin–orbit (SO) couplings in an ordinary GaAs/AlGaAs asymmetric double well, which favors the electron occupancy of three subbands $\nu = 1, 2, 3$. Resorting to an external gate, which adjusts the electron occupancy and the well symmetry, we demonstrate distinct three-level SO control of both Rashba (α_ν) and Dresselhaus (β_ν) intraband terms. Remarkably, as the gate varies, the first-subband SO parameters α_1 and β_1 comply with the usual linear behavior, while α_2 (β_2) and α_3 (β_3) respectively for the second and third subbands interchange the values, triggered by a gate controlled *band swapping*. This provides a pathway towards fascinating selective SO control in spintronic applications. Moreover, we observe that the interband Rashba ($\eta_{\mu\nu}$) and Dresselhaus ($\Gamma_{\mu\nu}$) terms also exhibit contrasting gate dependence. Our results should stimulate experiments probing SO couplings in multi-subband wells and adopting relevant SO features in future spintronic devices.

PACS: 71.70.Ej, 85.75.−d, 81.07.St DOI: 10.1088/0256-307X/37/11/117101

The spin–orbit (SO) interaction as a relativistic phenomenon has become of major relevance in the quest for spintronic devices as it provides a unique handle for electrical manipulation of the electron magnetic moment.[1,2] SO effects are of profound importance for a broad range of novel physical phenomena, such as spin textures,[3−6] spin Hall effects, topological insulators,[7] Majorana fermions,[8,9] and Weyl semimetals.[10] The SO coupling is also a key ingredient leading to intriguing *spin-valley locking* in 2D materials of transition metal dichalcogenides.[11−13] Our recent proposals of persistent skyrmion lattice,[14] stretchable spin helix[15] and of its symmetry breaking[16] also indicate the important role of SO effects in semiconductor nanostructures.

In GaAs quantum wells, the SO coupling has two dominant contributions: the Rashba[17] and Dressehaus[18] terms, arising from the structural and bulk inversion asymmetries, respectively. The Rashba coupling is linear and can be electrically controlled by using an external bias.[15,19−21] While the bulk Dresselhaus term is cubic, when projected into a quantized 2D system it retains a cubic component but also acquires a linear component, depending on the quantum confinement and the electron density,[15,22,23] respectively. In addition, the Rashba and Dressehaus SO fields exhibit distinct spintexures, in particular the Dresselhaus SO field in GaAs (110)-grown wells is unidirectional. As a consequence, the two SO effects often have distinct spintronic applications, e.g., Rashba effect for a spin field-effect transistor[24,25] and Dressehaus effect in (110)-grown quantum wells for the persistent spin helix state.[26] Notably, by combining the two SO effects and fine tuning them of equal strength, one can in principle achieve a non-ballistic spin field-effect transistor with a long spin lifetime.[26,27] The derivation and analyses of both the Rashba and Dresselhaus SO terms are given in a recent review by Xia *et al.*[28]

Extensive studies on the SO interaction have been devoted to semiconductor quantum wells with only one occupied electron subband.[3,4,15,21,22] Recently, quantum wells with two-subband electron occupancy have also drawn growing interest due to enriched physical phenomena arising from an additional orbital degree of freedom,[5,29−33] e.g., novel spin textures,[5] intrinsic spin Hall effect[31] and crossed spin helices.[14] However, despite substantial efforts, so far the SO features for a three-level quantum system, which is of profound importance in diverse subjects, e.g., quantum interference,[34] Kerr nonlinearity,[35] and optical

Supported by the National Natural Science Foundation of China (Grant Nos. 11874236 and 11004120), the QFNU Research Fund, and the Research Program of JNXY.
†These authors contributed equally to this work.
*Corresponding author. Email: yongjf@qfnu.edu.cn
© 2020 Chinese Physical Society and IOP Publishing Ltd

bistability and multistability,[36] still remains to be understood.

Here we consider a realistic GaAs/AlGaAs asymmetric double well, which is in favor of the electron occupancy of three subbands [Figs. 1(a) and 1(b)]. Resorting to an external gate potential, we demonstrate distinct gate control of the three-level SO couplings, including the Rashba and Dresselhaus terms of both intraband [Figs. 1(c) and 1(d)] and interband [Figs. 3(a) and 3(b)] kinds. Before discussing our self-consistent outcome (Fig. 2) for SO terms in detail, let us first introduce our model Hamiltonian.

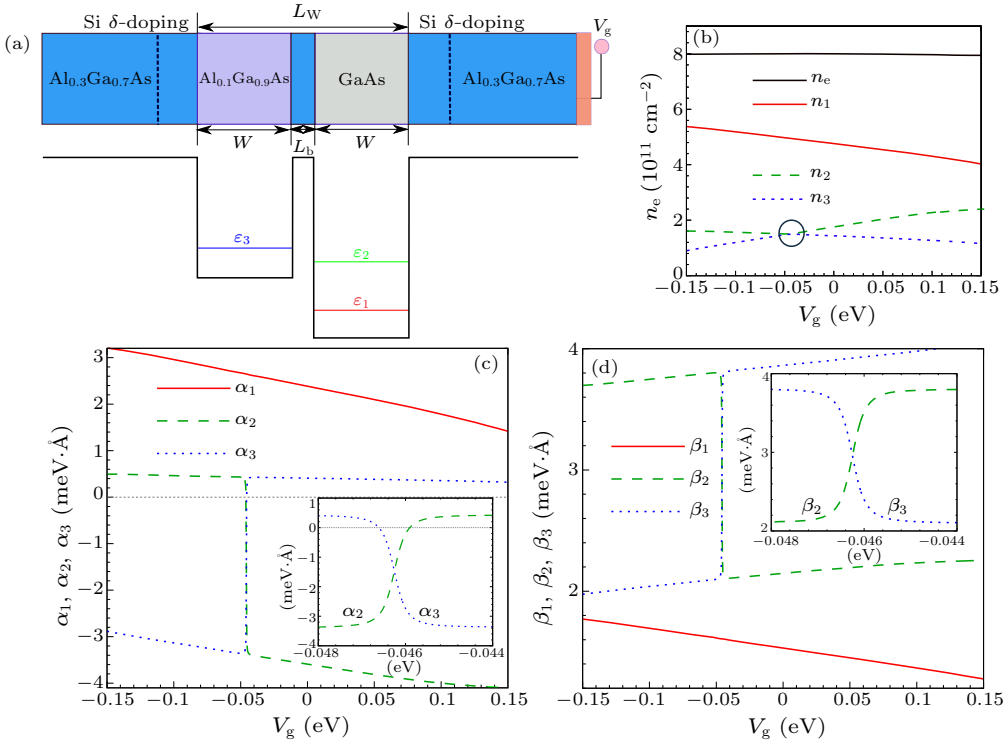

Fig. 1. (a) Upper: schematic diagram of a GaAs/AlGaAs asymmetric double well with L_w the overall width of the well; lower: structural potential profile of the well, where the horizontal red, green and blues lines inside the well indicate the subband energy levels $\mathcal{E}_1$, $\mathcal{E}_2$, and $\mathcal{E}_3$, respectively. An external gate potential V_g is adopted. (b) Dependence of the νth subband occupation n_ν on V_g with $n_e = n_1 + n_2 + n_3$. The black circle indicates where the second (n_2) and third (n_3) subbands are equally occupied. Rashba (c) and Dresselhaus (d) SO coefficients as functions of V_g, with the inset showing a blowup of the corresponding SO strength near $V_g = -0.0457$ eV.

Model Hamiltonians from 3D to 2D. We consider GaAs/AlGaAs quantum wells grown along the $z||[001]$ direction. Starting from the 8×8 Kane model[37,38] with both conduction and valence bands, one obtains via the folding down procedure[23,33] an effective 3D Hamiltonian only for conduction electrons,

$$\mathcal{H}^{3D} = \frac{\hbar^2 k^2}{2m^*} - \frac{\hbar^2}{2m^*}\frac{\partial^2}{\partial z^2} + V(z) + \mathcal{H}^{3D}_{\mathcal{R}} + \mathcal{H}^{3D}_{\mathcal{D}}, \quad (1)$$

where m^* is the electron effective mass and k is the in-plane electron momentum. The third term $V = V_w + V_g + V_d + V_e$ is the electron confining potential, which is determined self-consistently within the Poisson–Schrödinger–Hartree approximation, with V_w the structural potential (band offsets), V_g the external gate potential, V_d the doping potential, and V_e the electron Hartree potential.[14,15,23,33] For zero-bias self-consistent solutions including these potential contributions, see the Supplemental Material (SM). The terms $\mathcal{H}^{3D}_{\mathcal{R}}$ and $\mathcal{H}^{3D}_{\mathcal{D}}$ describe the Rashba and Dresselhaus SO interactions, respectively. The Rashba term reads $\mathcal{H}^{3D}_{\mathcal{R}} = \eta(z)(k_x\sigma_y - k_y\sigma_x)$, with $\eta(z) = \eta_w\partial_z V_w + \eta_H\partial_z(V_g + V_d + V_e)$ determining the Rashba strength and $\sigma_{x,y,z}$ the spin Pauli matrices. The parameters η_w and η_H involve bulk quantities of materials (we have assumed a universal value of η_w,[14,15,23] which in general differs at different interfaces).[23,33,39] The Dresselhaus contribution has the form $\mathcal{H}^{3D}_{\mathcal{D}} = \gamma[\sigma_x k_x(k_y^2 - k_z^2) + \text{c.c.}]$ with γ the bulk Dresselhaus parameter and $k_z = -i\partial_z$.[18,38]

Now we are ready to define an effective three-subband 2D model from the 3D Hamiltonian [Eq. 1]. We first determine (self-consistently) the spin-degenerate eigenvalues $\varepsilon_{\boldsymbol{k}\nu} = \mathcal{E}_\nu + \hbar^2 k^2/2m^*$ and the corresponding eigenspinors $|\boldsymbol{k}\nu\sigma\rangle = |\boldsymbol{k}\nu\rangle \otimes |\sigma\rangle$, $\langle \boldsymbol{r}|\boldsymbol{k}\nu\rangle = \exp(i\boldsymbol{k}\cdot\boldsymbol{r})\psi_\nu(z)$, of the well in the absence of SO interaction. Here we have defined $\mathcal{E}_\nu$ (ψ_ν), $\nu = 1, 2, 3$, as the ν-th quantized energy level (wave function) and $\sigma = \uparrow, \downarrow$ as the electron spin component along the z direction. Then the effective 2D Rashba model with three subbands in the coordi-

nate system $[x||(100),\ y||(010)]$ under the basis set $\{|\boldsymbol{k}1\uparrow\rangle, |\boldsymbol{k}1\downarrow\rangle, |\boldsymbol{k}2\uparrow\rangle, |\boldsymbol{k}2\downarrow\rangle, |\boldsymbol{k}3\uparrow\rangle, |\boldsymbol{k}3\downarrow\rangle\}$ reads

$$\mathcal{H}^{\rm 2D} = \begin{pmatrix} \rho_{11} & \rho_{12} & \rho_{13} \\ \rho_{21} & \rho_{22} & \rho_{23} \\ \rho_{31} & \rho_{32} & \rho_{33} \end{pmatrix}, \tag{2}$$

$$\begin{aligned}
\rho_{11} &= \varepsilon_{1,k}\mathbb{1} + \alpha_1(\sigma_y k_x - \sigma_x k_y) + \beta_1(\sigma_y k_y - \sigma_x k_x),\\
\rho_{12} &= \eta_{12}(\sigma_y k_x - \sigma_x k_y) + \Gamma_{12}(\sigma_y k_y - \sigma_x k_x),\\
\rho_{13} &= \eta_{13}(\sigma_y k_x - \sigma_x k_y) + \Gamma_{13}(\sigma_y k_y - \sigma_x k_x);\\
\rho_{21} &= \eta_{12}(\sigma_y k_x - \sigma_x k_y) + \Gamma_{12}(\sigma_y k_y - \sigma_x k_x),\\
\rho_{22} &= \varepsilon_{2,k}\mathbb{1} + \alpha_2(\sigma_y k_x - \sigma_x k_y) + \beta_2(\sigma_y k_y - \sigma_x k_x),\\
\rho_{23} &= \eta_{23}(\sigma_y k_x - \sigma_x k_y) + \Gamma_{23}(\sigma_y k_y - \sigma_x k_x);\\
\rho_{31} &= \eta_{13}(\sigma_y k_x - \sigma_x k_y) + \Gamma_{13}(\sigma_y k_y - \sigma_x k_x),\\
\rho_{32} &= \eta_{23}(\sigma_y k_x - \sigma_x k_y) + \Gamma_{23}(\sigma_y k_y - \sigma_x k_x),\\
\rho_{33} &= \varepsilon_{3,k}\mathbb{1} + \alpha_3(\sigma_y k_x - \sigma_x k_y) + \beta_3(\sigma_y k_y - \sigma_x k_x),
\end{aligned}$$

where $\sigma_{x,y}$ are the spin Pauli matrices, $\mathbb{1}$ the 2×2 matrix in both spin and orbital (subband) subspaces, $k_{x,y}$ the wave vector components along the $x \parallel [100]$ and $y \parallel [010]$ directions, and α_ν (β_ν), the Rashba (Dresselhaus) *intraband* couplings, respectively, for subbands $\nu = 1, 2, 3$. Note that Eq. (2) also accounts for the SO-induced *interband* couplings between subbands μ and ν via the parameters $\eta_{\mu\nu}$ (Rashba) and $\Gamma_{\mu\nu}$ (Dresselhaus), $\mu \neq \nu$.

Rashba and Dresselhaus SO Coefficients. The Rashba coefficients, Eq. (2), can be cast as the expectation values $\langle\cdots\rangle$ of the weighted derivatives of the potential contributions,

$$\eta_{\nu\nu'} = \langle\psi_\nu|\eta_{\rm w}\partial_z V_{\rm w} + \eta_{\rm H}\partial_z(V_{\rm g} + V_{\rm d} + V_{\rm e})|\psi_{\nu'}\rangle, \tag{3}$$

and the Dresselhaus strength SO reads

$$\Gamma_{\nu\nu'} = \gamma\langle\psi_\nu|k_z^2|\psi_{\nu'}\rangle, \tag{4}$$

where we have defined the intraband Rashba $\alpha_\nu \equiv \eta_{\nu\nu}$ and Dresselhaus $\beta_\nu \equiv \Gamma_{\nu\nu}$ as well as the interband Rashba $\eta_{\mu\nu}$ and Dressehaus $\Gamma_{\mu\nu}$, $\mu \neq \nu$. Note that the intraband Rashba term α_ν can be written in terms of several constituent contributions, i.e., $\alpha_\nu = \alpha_\nu^{\rm g} + \alpha_\nu^{\rm d} + \alpha_\nu^{\rm e} + \alpha_\nu^{\rm w}$, with $\alpha_\nu^{\rm g} = \eta_{\rm H}\langle\psi_\nu|\partial_z V_{\rm g}|\psi_\nu\rangle$ the gate contribution, $\alpha_\nu^{\rm d} = \eta_{\rm H}\langle\psi_\nu|\partial_z V_{\rm d}|\psi_\nu\rangle$ the doping contribution, $\alpha_\nu^{\rm e} = \eta_{\rm H}\langle\psi_\nu|\partial_z V_{\rm e}|\psi_\nu\rangle$ the electron Hartree contribution, and $\alpha_\nu^{\rm w} = \eta_{\rm w}\langle\psi_\nu|\partial_z V_{\rm w}|\psi_\nu\rangle$ the structural contribution. Similarly, the interband Rashba term $\eta_{\mu\nu} = \eta_{\mu\nu}^{\rm g} + \eta_{\mu\nu}^{\rm d} + \eta_{\mu\nu}^{\rm e} + \eta_{\mu\nu}^{\rm w}$. For convenience, we also use $\alpha_\nu^{\rm g+d} = \alpha_\nu^{\rm g} + \alpha_\nu^{\rm d}$ and $\eta_{\mu\nu}^{\rm g+d} = \eta_{\mu\nu}^{\rm g} + \eta_{\mu\nu}^{\rm d}$. Even though α_ν and $\eta_{\mu\nu}$ comprise seemingly independent contributions, we note that each of them depends on the total potential via the self-consistent wave function.

System and Parameters. The system we consider is similar to the experimental sample of Ref. [3]: the [001]-grown GaAs wells sandwiched between 48-nm $Al_{0.3}Ga_{0.7}As$ barriers (the samples in Ref. [3] consist of ten quantum wells; we only consider a single well in our simulation since electrons are entirely confined in one of the wells), while with an additional $Al_{0.1}Ga_{0.9}As$ layer and a central barrier $Al_{0.3}Ga_{0.7}As$ layer embedded in the GaAs layer to form an asymmetric double well, Fig. 1(a), favoring the electron occupancy of three subbands. We consider the overall width of the well $L_{\rm w} = 60\,$nm and the width of the central barrier $L_{\rm b} = 6\,$nm. The left ($Al_{0.1}Ga_{0.9}As$) and right (GaAs) wells are assumed having the same width of $w = 27\,$nm.

The overall areal electron density $n_e = 8.0 \times 10^{11}\,{\rm cm}^{-2}$, arising from the delta doping (Si) layers symmetrically sitting 47 nm away from the center of the structure, is adopted from experimental measurements.[3] The temperature is held fixed at $T = 75\,$K (the temperature goes into our self-consistent simulation through the Fermi–Dirac distribution).[3] We consider the Rashba parameters $\eta_w = 3.97\,\text{Å}^2$ and $\eta_H = -5.30\,\text{Å}^2$ that we recently obtained for GaAs wells,[15,23] Eq. (3). The bulk Dresselhaus constant is chosen as $\gamma = 11.0\,{\rm eV}\cdot\text{Å}^3$, Eq. (4), extracted together with our experimental collaborators via a realistic fitting procedure for a set of wells of different widths.[15,23] Note that this value is also in agreement with the one obtained in a recent study by Walser *et al.*[22]

Distinct SO Control. We perform a detailed self-consistent calculation by solving the Schrödinger and Poisson coupled equations within the Hartree approximation.[15,23] Before discussing the SO terms in detail, we first have a look at our self-consistent outcome of how an external gate alters electron subband occupations n_ν, as shown in Fig. 1(b). The overall electron density is held fixed at $n_e = 8 \times 10^{11}\,{\rm cm}^{-2}$ with $n_e = n_1 + n_2 + n_3$ in the whole gate ranges considered, indicating that the fourth subband maintains empty. As $V_{\rm g}$ increases, while the first-subband occupation (n_1) constantly decreases, we find that the occupations of the second (n_2) and third (n_3) subbands exhibit opposite gate dependence and become essentially the same (i.e., $n_2 = n_3$) at $V_{\rm g} = -0.0457\,$eV, see the black circle in Fig. 1(b). The matching second- and third-subband occupations imply that the subband energy levels $\mathcal{E}_2$ and $\mathcal{E}_3$ turn to degenerate when $V_{\rm g} = -0.0457\,$eV and for even larger value of $V_{\rm g}$ the order of the two levels is inevitably interchanged. The emergent band swapping when $V_{\rm g}$ alters is the main source giving rise to distinct SO control for the three-level quantum system, as we analyze next.

In Fig. 1(c), we show the Rashba coefficients of the three subbands as functions of $V_{\rm g}$. Remarkably, we observe distinct gate dependence of them. Specifically, the first-subband Rashba strength α_1 essentially obeys

the linear behavior, as anticipated, and consistently decreases with increasing V_g. In contrast, the Rashba coefficients of the second (α_2) and third (α_3) subbands have opposite signs, and they interchange the values across $V_g = -0.0457$ eV. The inset shows a blowup of the crossover between α_2 and α_3. For distinct constituent contributions, i.e., $\alpha_\nu^{e,w,g+d}$, to the intraband Rashba SO couplings, see the SM. Concerning the Dresselhaus terms, while β_1, β_2 and β_3 of the three subbands have the same sign, their gate dependence is similar to that of Rashba, as shown in Fig. 1(d). To elucidate the underlying physics, we resort to our self-consistent outcome for the electron confining potential V_{sc} and the wave functions ψ_ν.

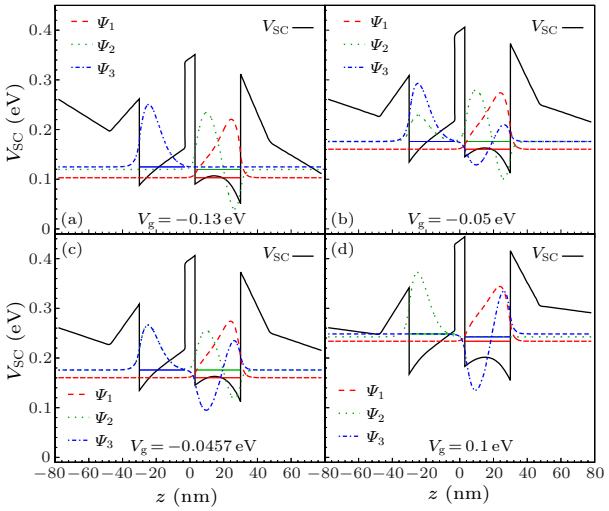

Fig. 2. Self-consistent potential (V_{sc}) and the corresponding wave function profiles of the first (ψ_1), second (ψ_2) and third (ψ_3) subbands for a GaAs/AlGaAs double well, at $V_g = -0.13$ (a), -0.05 (b), -0.0457 (c), and 0.1 eV (d). The horizontal red, green, and blues lines inside the well indicate the subband energy levels $\mathcal{E}_1$, $\mathcal{E}_2$, and $\mathcal{E}_3$, respectively.

Figures 2(a)–2(d) show the self-consistent potential and wave functions of the three subbands for our well at $V_g = -0.13$, -0.05, -0.0457, and 0.1 eV, respectively. For a lower value of $V_g = -0.13$ eV, it is found that electrons occupying the first and second subbands are mostly confined in the right well, while for the third subband electrons preferably reside in the left well, see the wave functions ψ_1, ψ_2 and ψ_3. This configuration of the three energy levels corresponds to exactly the geometry illustrated in the lower panel of Fig. 1(a). As V_g increases, the gate shall lift up the potential energy of the overall system. Since the gate is applied on the right of the structure [Fig. 1(a)], electrons confined in the right well react more sensitively in energy increment than those localized in the left well. As a consequence, the energy level separation between $\mathcal{E}_2$ and $\mathcal{E}_3$ shrinks with growing V_g and become basically degenerate near $V_g = -0.0457$ eV. Then, for even larger V_g the aforementioned band swapping naturally follows.

From electron distributions across the left and right wells, we can more vividly see the occurrence of band swapping. When V_g increases, we find that the second-subband electrons (ψ_2) are apt to *move* from the left well to the right one, while for the third subband (ψ_3) the scenario is reversed (i.e., from right to left), see Figs. 2(a)–2(d). We should note that the wave function profiles of ψ_2 and ψ_3 near $V_g = -0.0457$ eV are very similar and are largely overlapped, see Fig. 2(c). This straightforwardly follows from the essential degeneracy between the subband energy levels $\mathcal{E}_2$ and $\mathcal{E}_3$.

So far, it is clear that the intriguing feature of the Rashba α_2 and α_3 interchanging the values when we adjust V_g, similarly for the Dresselhaus β_2 and β_3, Figs. 1(c) and 1(d), straightforwardly arises from the occurrence of band swapping.

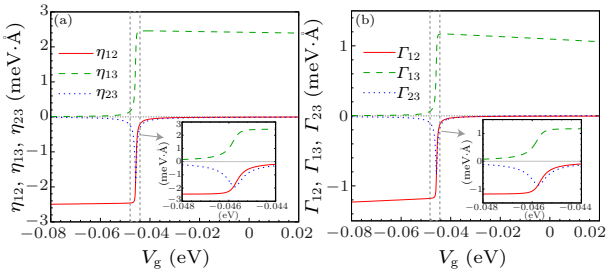

Fig. 3. Interband Rashba $\eta_{\mu\nu}$ (a) and Dresselhaus $\Gamma_{\mu\nu}$ (b) SO coefficients as functions of V_g. The insets show a blowup of the corresponding SO strengths near $V_g = -0.0457$ eV.

Now we turn to the interband Rashba ($\eta_{\mu\nu}$) and Dresselhaus ($\Gamma_{\mu\nu}$) SO couplings, as shown in Figs. 3(a) and 3(b), respectively. We first look at the interband SO terms between the second and third subbands, which involve the band swapping across $V_g = -0.0457$ eV. We observe that both η_{23} and Γ_{23} achieve their maximal strengths at $V_g = -0.0457$ eV. This arises from the interband SO terms depending on the overlap of the wave functions of the two subbands, see Eqs. (3) and (4). Near $V_g = -0.0457$ eV, an essential degeneracy of $\mathcal{E}_2 = \mathcal{E}_3$ emerges and hence ψ_2 and ψ_3 have a perfect overlap [Fig. 2(c)]. However, away from the degeneracy point, ψ_2 and ψ_3 are largely separated [Figs. 2(a) and 2(d)], i.e., one is mostly confined in the left well and the other in the right one.

On the other hand, the interband SO terms concerning the first with either the second or third subband, i.e., η_{12} (Γ_{12}) and η_{13} (Γ_{13}), display distinctly contrasting behavior of gate dependence, as compared to η_{23} and Γ_{23}. Specifically, η_{12} and Γ_{12} remain independent of the gate for lower values of V_g, while they vanish across $V_g = -0.0457$ eV. As for η_{13} and Γ_{13}, the behavior is the opposite, i.e., they are basically zero for lower V_g while rise abruptly across the band swapping point at $V_g = -0.0457$ eV. Even though the gate

control of η_{23} (Γ_{23}) is in stark contrast with that of η_{12} (Γ_{12}) and η_{13} (Γ_{13}), we should emphasize that the latter interband terms are also primarily determined by the overlap of the corresponding wave functions. The first and second (third) subbands are largely overlapped (separated) when $V_{\rm g}$ is lower than $-0.0457\,$eV, while are mostly separated (overlapped) otherwise, see Figs. 2(a) and 2(d). This follows how the interband SO coefficients η_{12} (Γ_{12}) and η_{13} (Γ_{13}) depend on $V_{\rm g}$. For the gate dependence of several constituent contributions to interband Rashba terms, i.e., $\eta_{\mu\nu}^{\rm e,w,g+d}$, see the SM.

In summary, we have investigated the Rashba and Dresselhaus spin–orbit couplings in a realistic GaAs/AlGaAs asymmetric double well favoring the electron occupancy of three subbands. We have demonstrated distinct gate control of the three-level SO terms, primarily arising from the emergence of band swapping. This opens a pathway towards selective SO gate control as the electron eigenstates can be experimentally probed,[40] greatly fascinating for spintronic applications. The interband SO couplings also display contrasting gate dependence. Although only the band swapping between the second and third subbands, which pertain to the right or left well, occurs in the parameter range considered, we note that a band swapping involving the first subband may also emerge for an even larger value of gate potential. Here we did not consider the latter case as the fourth subband in this scenario starts to be occupied. Our results are expected to stimulate experiments for probing SO couplings in quantum wells with multiple occupancy and for adopting relevant SO features in future spintronic devices.

References

[1] Awschalom D, Loss D and Samarth N 2002 *Semiconductor Spintronics and Quantum Computation* (New York: Springer)
[2] Žutić I, Fabian J and Sarma S D 2004 *Rev. Mod. Phys.* **76** 323
[3] Koralek J D, Weber C P, Orenstein J, Bernevig B A, Zhang S C, Mack S and Awschalom D D 2009 *Nature* **458** 610
[4] Walser M P, Reichl C, Wegscheider W and Salis G 2012 *Nat. Phys.* **8** 757
[5] Bentmann H, Abdelouahed S, Mulazzi M, Henk J and Reinert F 2012 *Phys. Rev. Lett.* **108** 196801
[6] Noguchi K, Kuroda R, Yaji K, Kobayashi K, Sakano M, Harasawa A, Kondo T, Komori F and Shin S 2017 *Phys. Rev. B* **95** 041111(R)
[7] Bernevig B A, Hughes T L and Zhang S C 2006 *Science* **314** 1757
[8] Lutchyn R M, Sau J D and Sarma S D 2010 *Phys. Rev. Lett.* **105** 077001
[9] Oreg G, Refael Y and Oppen F V 2010 *Phys. Rev. Lett.* **105** 177002
[10] Weng H M, Fang C, Fang Z, Bernevig B A and Dai X 2015 *Phys. Rev. X* **5** 011029
[11] Xiao D, Liu G B, Feng W X, Xu X D and Yao W 2012 *Phys. Rev. Lett.* **108** 196802
[12] Fu J Y, Bezerra A and Qu F Y 2018 *Phys. Rev. B* **97** 115425
[13] Fu J Y, Cruz J M R and Qu F Y 2019 *Appl. Phys. Lett.* **115** 082101
[14] Fu J Y, Penteado P H, Hachiya M O, Loss D and Egues J C 2016 *Phys. Rev. Lett.* **117** 226401
[15] Dettwiler F, Fu J Y, Mack S, Weigele P J, Egues J C, Awschalom D D and Zumbühl D M 2017 *Phys. Rev. X* **7** 031010
[16] Weigele P J, Marinescu D C, Dettwiler F, Fu J Y, Mack S and Egues J C 2020 *Phys. Rev. B* **101** 035414
[17] Bychkov Y A and Rashba E I 1984 *JETP Lett.* **39** 78
[18] Dresselhaus G 1955 *Phys. Rev.* **100** 580
[19] Nitta J, Akazaki T, Takayanagi H and Enoki T 1997 *Phys. Rev. Lett.* **78** 1335
[20] Studer M, Salis G, Ensslin K, Driscoll D C and Gossard A C 2009 *Phys. Rev. Lett.* **103** 027201
[21] Sasaki A, Nonaka S, Kunihashi Y, Kohda M, Bauernfeind T, Dollinger T, Richter K and Nitta J 2014 *Nat. Nanotechnol.* **9** 703
[22] Walser M P, Siegenthaler U, Lechner V, Schuh D, Ganichev S D, Wegscheider W and Salis G 2012 *Phys. Rev. B* **86** 195309
[23] Fu J Y and Egues J C 2015 *Phys. Rev. B* **91** 075408
[24] Datta S and Das B 1990 *Appl. Phys. Lett.* **56** 665
[25] Chuang P, Ho S, Smith L W, Sfigakis F, Pepper M, Chen C, Fan J, Griffiths J P, Farrer I, Beere H E, Jones G A C, Ritchie D A and Chen T 2015 *Nat. Nanotechnol.* **10** 35
[26] Bernevig B, Orenstein J and Zhang S C 2006 *Phys. Rev. Lett.* **97** 236601
[27] Schliemann J, Egues J C and Loss D 2003 *Phys. Rev. Lett.* **90** 146801
[28] Xia J B, Ge W K and Chang K 2012 *Semiconductor Spintronics* (Beijing: Science Press) (in Chinese)
[29] Hu C M, Nitta J, Akazaki T, Takayanagi H, Osaka J, Pfeffer P and Zawadzki W 1999 *Phys. Rev. B* **60** 7736
[30] Hu C M, Nitta J, Akazaki T, Takayanagi H, Osaka J, Pfeffer P and Zawadzki W 2000 *Physica E* **6** 767
[31] Hernandez F G G, Nunes L, Gusev G and Bakarov A 2013 *Phys. Rev. B* **88** 161305(R)
[32] de Andrada e Silva E A, La Rocca G C and Bassani F 1997 *Phys. Rev. B* **55** 16293
[33] Calsaverini R S, Bernardes E, Egues J C and Loss D 2008 *Phys. Rev. B* **78** 155313
[34] Derkacz L and Jakóbczyk L 2006 *Phys. Rev. A* **74** 032313
[35] Sun H, Gong S Q, Niu Y P, Jin S Q, Li R X and Xu Z Z 2006 *Phys. Rev. B* **74** 155314
[36] Joshi A and Xiao M 2003 *Phys. Rev. Lett.* **91** 143904
[37] Kane E Q 1957 *J. Phys. Chem. Solids* **1** 249
[38] Winkler R 2003 *Spin-Orbit Coupling Effects in Two-Dimensional Electron and Hole Systems* (New York: Springer)
[39] Wang W, Li X M and Fu J Y 2015 *J. Magn. Magn. Mater.* **411** 84
[40] Marzin J V and Gérard J M 1989 *Phys. Rev. Lett.* **62** 2172

Supplementary Material

Distinct three-level spin-orbit control associated with electrically controlled band swapping

Yu Suo (索育),[1,2,*] Hao Yang (杨浩),[1,*] and Jiyong Fu (付吉永)[1,3,4,†]

[1] *Department of Physics, Qufu Normal University, 273165 Qufu, Shandong, China*

[2] *Department of Physics, Jining University, 273155 Qufu, Shandong, China*

[3] *Instituto de Física, Universidade de Brasília, Brasília-DF 70919-970, Brazil*

[4] *Collaborative Innovation Center of Light Manipulations and Applications, Shandong Normal University, Jinan 250358, China*

* These authors contributed equally to this work.

† yongjf@qfnu.edu.cn

I. ZERO BIAS SELF-CONSISTENT SOLUTIONS

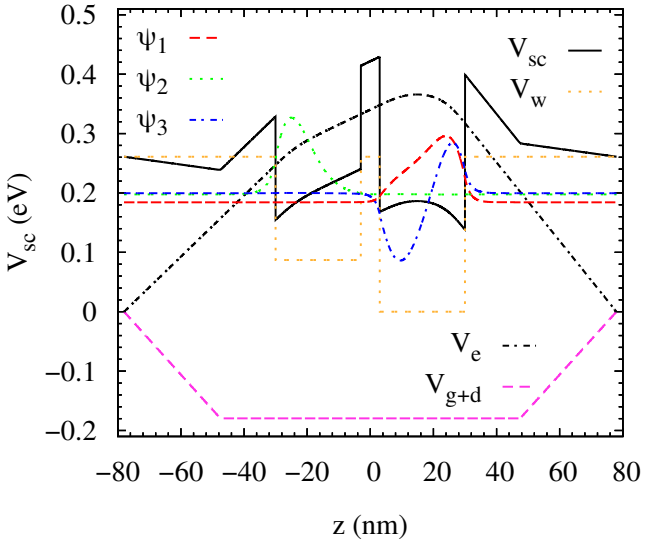

Figure S1. Self-consistent potential $V_{\rm sc}$ including its several constituent contributions as well as the corresponding wave function profiles ψ_1, ψ_2 and ψ_3 of three subbands for our GaAs/AlGaAs double well at $V_{\rm g} = 0$. These constituent potential contributions contain the quantum well band-offset potential $V_{\rm w}$, the electron Hartree potential $V_{\rm e}$, and the gate plus doping potential $V_{\rm g+d}$. The three subband energy levels are $\mathcal{E}_1 = 184.32$ meV, $\mathcal{E}_2 = 197.62$ meV, and $\mathcal{E}_3 = 199.59$ meV. The electron density is held fixed at $n_e = 8.0 \cdot 10^{11}{\rm cm}^{-2}$. The resulting Fermi energy is $\mathcal{E}_{\rm F} = 200.83$ meV. The fourth subband is about 27 meV above $\mathcal{E}_{\rm F}$, indicating it is unoccupied.

Figure S1 shows the self-consistent potential and the corresponding wave function profiles of three subbands for our GaAs/AlGaAs double well at $V_{\rm g} = 0$. In the parameter range considered, at zero bias, electrons of the first, second, and third subbands are largely localized in the right, left, and right wells, respectively, cf. Figs. S1 and Fig. (2) of the main text. Note that gate plus doping potential $V_{\rm g+d}$ maintains flat across the whole region having electron distributions (i.e., -40 nm $< z <$ 40 nm), because of the symmetric doping condition we adopted, see the main text.

II. CONSITUENT CONTRIBUTIONS TO RASHBA SO COUPLINGS

We show several distinct contributions to the Rashba SO couplings. Below we consider the intraband Rashba terms in Sec. II A and the interband ones in Sec. II B.

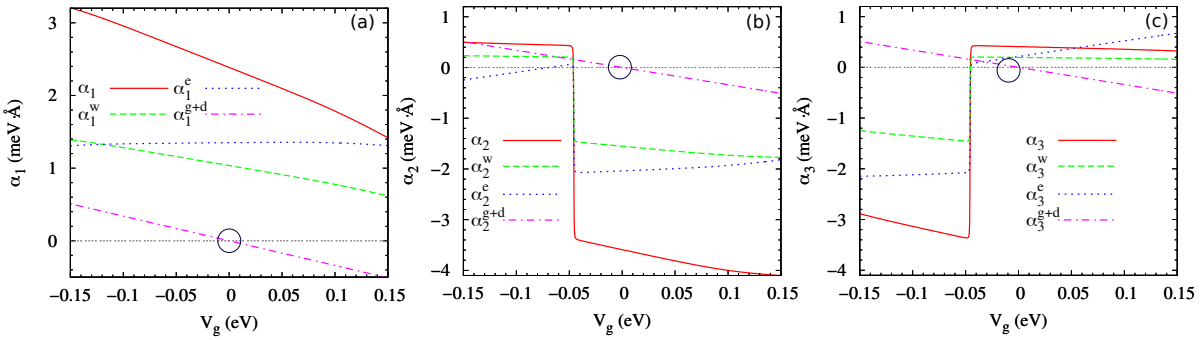

Figure S2. Distinct contributions to Rashba strengths of the first α_1 (a), second α_2 (b), and third α_3 (c) subbands as functions of V_g. These include the gate plus doping contribution α_ν^{g+d}, the electron Hartree contribution α_ν^e, and the structural contribution α_ν^w, with $\alpha_\nu = \alpha_\nu^e + \alpha_\nu^{g+d} + \alpha_\nu^w$. The black circles indicate that α_ν^{g+d} for all three subbands identically vanishes at $V_g = 0$.

A. Intraband Rashba terms

In Fig. S2, we show the intraband Rashba coefficients α_ν of the three subbands and the corresponding constituent contributions as functions of V_g. For the electron Hartree contribution α_ν^e, the first subband α_1^e maintains essentially constant as V_g varies [Fig. S2(a)], since the first-subband electrons are kept in the right well in the whole gate ranges (see Fig. 2 of the main text). In contrast, for the second [Fig. S2(b)] and third [Fig. S2(c)] subbands, α_2^e and α_3^e basically interchange the values near $V_g = -0.0457$ eV, at which the band swapping of the two subbands occurs. Concerning the structural contribution α_ν^w, it is found that α_1^w displays basically the linear behavior with V_g, while α_2^w and α_3^w interchange the values when we adjust V_g, similar to the electron Hartree contributions α_2^e and α_3^e. As for the gate plus doping contribution α_ν^{g+d}, it exhibits linear gate dependence for all three subbands, due to the linear characteristic of the gate potential we adopted [1–5].

Note that, at zero bias $V_g = 0$, even though the overall α_ν is nonzero because of the *intrinsic* structual inversion asymmetry between the right and left wells of the system (Fig. 1 of the main text), α_ν^{g+d} identically vanishes for all three subbands, as indicated by the black circles. This straightforwardly follows from the fact that the gate plus doping potential V_{g+d} is basically z independent ("flat" characteristic aforementioned) across the region where there are electron distributions, see Fig. S1 and Sec. I. A uniform V_{g+d} near the well regions leads to the zero force field of the gate plus doping potential, i.e., $\partial_z V_{g+d} = 0$, and so the vanishing Rashba contribution α_ν^{g+d}, see Eq. (3) of the main text.

B. Interband Rashba terms

Figure S3 shows the gate dependence of interband Rashba coefficients and the corresponding constituent contributions. For the electron Hartree contribution $\eta^{\rm e}_{\mu\nu}$ and the structural contribution $\eta^{\rm w}_{\mu\nu}$, we find that near $V_{\rm g} = -0.0457$ eV, $\eta^{\rm e,w}_{12}$ and $\eta^{\rm e,w}_{13}$ basically interchange the values while $\eta^{\rm e,w}_{23}$ exhibits a resonance, follows from the band swapping between the second and third subbands. We should emphasize that $\eta^{\rm g+d}_{\mu\nu}$ maintains zero in the whole gate ranges because of the orthogonality condition between distinct subbands μ and ν, cf. Figs. S3(a)-S3(c).

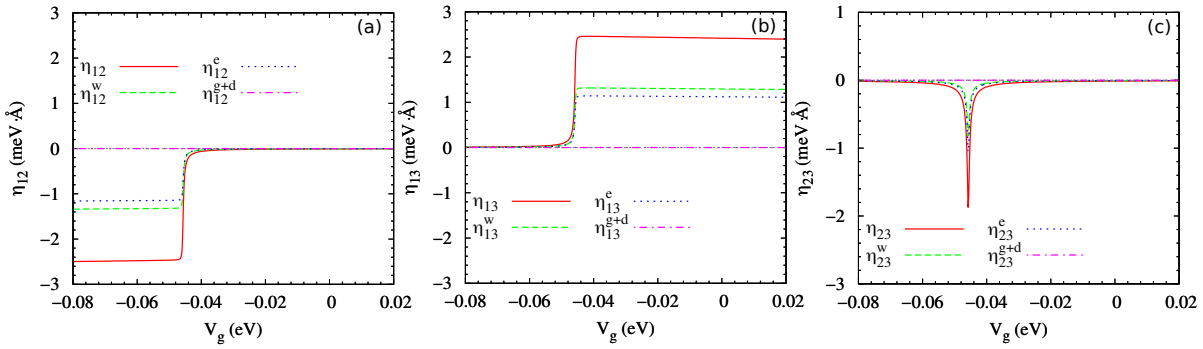

Figure S3. Interband Rashba coefficients $\eta_{\mu\nu}$ between subbands μ and ν ($\mu \neq \nu$) and its several constituent contributions: the gate plus doping $\eta^{\rm g+d}_{\mu\nu}$, the electron Hartree $\eta^{\rm e}_{\mu\nu}$, and the structural $\eta^{\rm w}_{\mu\nu}$ contributions with $\eta_{\mu\nu} = \eta^{\rm e}_{\mu\nu} + \eta^{\rm g+d}_{\mu\nu} + \eta^{\rm w}_{\mu\nu}$ as functions of $V_{\rm g}$. (a) η_{12}, (b) η_{13}, and (c) η_{23}.

[1] E. Bernardes, J. Schliemann, M. Lee, J. C. Egues, and D. Loss, Spin-orbit interaction in symmetric wells with two subbands, Phys. Rev. Lett. **99**, 076603 (2007).

[2] R. S. Calsaverini, E. Bernardes, J. C. Egues, and D. Loss, Intersubband-induced spin-orbit interaction in quantum wells, Phys. Rev. B **78**, 155313 (2008).

[3] J. Y. Fu and J. C. Egues, Spin-orbit interaction in GaAs wells: From one to two subbands, Phys. Rev. B **91**, 075408 (2015).

[4] J. Y. Fu, P. H. Penteado, M. O. Hachiya, D. Loss, and J. C. Egues, Persistent skyrmion lattice of noninteracting electrons with spin-orbit coupling, Phys. Rev. Lett. **117**, 226401 (2016).

[5] F. Dettwiler, J. Y. Fu, S. Mack, P. J. Weigele, J. C. Egues, D. D. Awschalom, and D. M. Zumbühl, Stretchable persistent spin helices in GaAs quantum wells, Phys. Rev. X **7**, 031010 (2017).